ESO observing programme: Fornax 3D galaxy survey (F3D)

Abstract

The F3D is an integral field spectroscopic survey of the Fornax cluster of galaxies, that targets galaxies brighter than μ_B=15 and within the virial radius of the cluster (Rv ~ 0.7 Mpc, Drinkwater et al. 2001). The survey was conducted with the Multi Unit Spectroscopic Explorer (MUSE, Bacon et al. 2010) at the Unit Telescope 4 of the Very Large Telescope. The survey design and first results are described in Sarzi et al. (2018). The complete set of maps for the stellar and ionized-gas kinematics as well as for the stellar population and gas properties obtained from the survey is described in Iodice et al. (2019), and they are based on this data release (F3D-DR1). The main scientific goals of the survey are:

- Understand the assembly history of the Fornax cluster, through the characterization of the main properties of the galaxies within its Virial radius.
- Understand the formation and the merger history of the Early-Type Galaxies (ETGs), through a detailed analysis of their stellar kinematic and stellar population properties aided by state-of-the-art chemo-dynamical modelling.
- Understand the formation of substructures in galaxies, such as kinematically decoupled components, nuclear disks and star clusters, thin and thick stellar disks even when deeply embedded in the main body of a galaxy and extended stellar halos.
- Study the properties of globular cluster and planetary nebulae population in order to further constrain their formation mechanisms and aid the three-dimensional mapping of the Fornax cluster through distance measurement of individual galaxies.

Overview of observations

The 31 survey targets of DR1 and their basic properties are listed in Table 1. The MUSE observations were carried out in service mode between July 2016 and December 2017 under the program ID 296.B-5054(A). The wide-field mode ensured a field of view of 1×1 arcmin^2 with a spatial sampling of 0.2×0.2 arcsec^2. The wavelength range from 4650 to 9300 Å was covered with a spectral sampling of 1.25 Å pixel^{-1} and a nominal spectral resolution of FWHM inst = 2.5 Å at 7000 Å.

Each galaxy was observed with several different pointings (from 1 to 3), depending on its extent on sky. The total integration times for the central and middle pointings are about 1 h, while an integration of 1.5h was necessary to reach the limiting surface brightness of μ_B= 25 mag arcsec^{-2} in the outer pointings. A dither of a few arcseconds and a rotation by 90° were applied to the single exposures, in order to minimize the signature of the 24 MUSE slices on the field of view. Except for pointings encompassing rather small objects compared to the MUSE field of view, sky frames were acquired immediately before/after each science exposure in order to perform sky modelling and subtraction on the single spaxels. The observations were done in good seeing conditions with a median FWHM = 0.72 arcsec, according to the DIMM seeing measurements taken at the beginning of the observation.

Release Content

The DR1 of F3D consists of 31 datacubes files and 31 white-lamp images. The total data volume is ~122 GB. The target list and their basic properties from the literature is provided in **Table 1**.

NAME	RA (J2000)	DEC (J2000)	Type	cz	m_B	R_e	R_{25}	μ_B (30")
	hh:mm:ss.s	+/- dd:mm:ss		km s^{-1}	mag	arcmin	arcmin	mag $arcsec^{-2}$
FCC 83	03:30:35.1	−34:51:14	E5	1543	12.3	0.46	1.5a	22.7
FCC 90	03:31:08.1	−36:17:19	E4 pec	1916	15	0.2	0.5a	25.1
FCC 113	03:33:06.8	−34:48:26	ScdIII pec	1553	15.2	0.25	0.6b	...
FCC 119	03:33:33.7	−33:34:18	S0 pec	1554	15	0.29	0.4a	25.5
FCC 143	03:34:59.1	−35:10:10	E3	1376	14.3	0.16	0.5a	25
FCC 147	03:35:16.8	−35:13:34	E0	1386	11.9	0.42	1.3a	22.6
FCC 148	03:35:16.8	−35:15:56	S0	730	13.6	0.25	1.1a	22.7
FCC 153	03:35:30.9	−34:26:45	S0	1639	13	0.19	1.3b	21.2
FCC 161	03:36:04.0	−35:26:30	E0	1405	11.7	0.39	2.7a	22.6
FCC 167	03:36:27.5	−34:58:31	S0/a	1827	11.3	0.62	2.0a	21.1
FCC 170	03:36:31.6	−35:17:43	S0	1793	13	0.23	1.3a	21.2
FCC 176	03:36:45.0	−36:15:17	Sba	1465	13.7	0.43	0.8b	...
FCC 177	03:36:47.4	−34:44:17	S0	1495	13.2	0.25	1.2a	21.6
FCC 179	03:36:46.3	−35:59:57	Sa	839	12.4	...	1.7b	...
FCC 182	03:36:54.3	−35:22:23	SB0 pec	1823	14.9	0.19	0.6b	≥25.0
FCC 184	03:36:56.9	−35:30:24	SB0	1337	12.3	0.83	1.8b	21.1
FCC 190	03:37:08.9	−35:11:37	SB0	1784	13.5	0.27	0.8b	24
FCC 193	03:37:11.7	−35:44:40	SB0	999	12.8	0.33	1.4b	21.9
FCC 219	03:38:52.1	−35:35:38	E2	1944	10.9	0.41	2.1a	21.6
FCC 249	03:40:41.9	−37:30:33	E0	1521	13.6	0.16	0.6a	24.7
FCC 255	03:41:03.4	−33:46:38	S0	1217	13.7	0.23	1.0b	20.4
FCC 263	03:41:32.2	−34:53:17	SBcdIII	1708	14.6	0.34	0.8b	...
FCC 276	03:42:19.2	−35:23:36	E4	1454	11.8	0.54	1.6a	22.2
FCC 277	03:42:22.6	−35:09:10	E5	1620	13.8	0.16	0.7a	24.1
FCC 285	03:43:01.8	−36:16:11	SdIII	895	14.2	0.48	1.0b	...
FCC 290	03:43:37.0	−35:51:13	ScII	1217	12.8	...	1.5b	...
FCC 301	03:45:03.5	−35:58:17	E4	1020	14.2	0.17	0.5a	24.9
FCC 306	03:45:45.3	−36:20:40	SBmII	–	15.6	...	0.3b	...
FCC 308	03:45:54.7	−36:21:25	Sd	–	13.8	0.06	1.3b	...
FCC 310	03:46:13.7	−36:41:43	SB0	1352	13.5	0.43	0.9b	20
FCC 312	03:46:18.9	−34:56:31	Scd	1932	13.5	...	2.4b	...

Table 1: Target list of the F3D DR1. In column 1 is given the target name. In columns 2 and 3 are listed the J2000 celestial coordinates. Columns from 4 to 7 indicates, respectively: Morphological type, heliocentric radial velocity, total B-band magnitude, and B-band effective radius from Ferguson & Sandage (1989). Column 8 shows the semi-major axis of the best-fitting ellipse to the isophote at μB = 25 mag arcsec−2 (from a: Caon et al. 1994 or b: de Vaucouleurs et al. 1991). Column 9 reports the B-band surface brightness level at R = 30 arcsec (from Caon et al. 1994). Column 9 reports the number of pointigs the galaxy was observed. Missing entries in the table refer to values that are unavailable in the cited references.

Release Notes

Data Reduction and Calibration

The data reduction was performed with the MUSE pipeline version 2.2 (Weilbacher et al. 2012, 2016) under the ESOREFLEX environment (Freudling et al. 2013). The main steps included bias and overscan subtraction, flat fielding to correct the pixel-to-pixel response variation, wavelength calibration, determination of the line spread function, and illumination correction. By using the dedicated sky frames, the sky subtraction was done by fitting and subtracting a sky model spectrum on each spaxel of the field of view. The flux calibration and the first-order correction of the atmospheric telluric features were obtained using the spectro-photometric standard star observed at twilight. For each galaxy of the sample, the exposures in each single pointings were aligned using reference stars and then combined. Residual sky contribution on each individual combined pointing was evaluated by means of principle component analysis (ZAP, Soto et al, 2016) using either the dedicated sky datacube as reference (for targets or pointings where the target contribution was relevant across all the field of view), or the datacube itself (for targets or pointing where there was enough empty sky regions, where the contribution of the target was irrelevant).

For galaxies that require more than one single pointing, the individual pointings were aligned and then combined together to produce the final MUSE mosaics according to the following procedure:

- The data cube for each pointing was integrated along wavelength assuming the transmission of the SLOAN r-band filter.
- R-band images were astrometrically aligned using a reference image from FDS (Fornax Deep Survey, Iodice et al. 2019). Bright sources in the field of view of the reference image and the r-band images obtained from the data cubes were used for alignment.
- The surface brightness profiles on a pseudo-slit of 5" width aligned along the galaxy major axis were obtained from each aligned r-band image and the reference image.
- Each r-band image was multiplied by a factor to match the surface brightness profile of the reference image. Multiplicative factors were calculated by means of a least-square minimization.
- The data cubes of each pointing were spatially aligned (this step implied a liner interpolation of the data cubes) using the same offsets in RA and DEC calculated to align the r-band images to the reference VISTA image, scaled by the multiplicative factor and then combined. During combination, we masked a region 3 pixels wide around each field of view, in order to minimize contamination from border vignetting.

For galaxies that require only one single pointing, the datacube was multiplied by a factor to match the major axis pseudo-slit profile with that of the reference image, as done for the multiple-pointing targets. These mosaics (either single or multiple pointings) map the galaxy structure and stellar population out to 2–3 Re for the ETGs and out to 1–2 Re for the LTGs.

Data quality and known issues

Spectral resolution

The effective spectral resolution was measured by cross-correlating sky twilight cubes with an high resolution solar spectrum. Twilight cubes were obtained by combining individual twilight

exposures following the same observation pattern as the target galaxies, including rotations and offsets. The cross-correlation with solar template was performed on several wavelength regions, to measure the variation with wavelength. The measured spectral resolution was on average FWHM_inst = 2.8 Å with little variation (<0.2 Å) with wavelength and position over the field of view. This is slightly larger than the nominal value due to the combination of different offset exposures taken at different position angles.

Astrometric precision

The relative position between different exposures after alignment is precise up to ~1/3 pixels (0.08"). This was measured from the position of the centroids of the reference sources used for alignment (after the alignment). The final astrometric solution of the final mosaic were not corrected using reference catalogs (e.g. USNO-B or GAIA), therefore there is an uncertainty on the absolute coordinates that is compatible with the telescope pointing precision (about 5 arcec, in the worst case).

Spectral quality, depth of observation, signal-to-noise.

Each datacube indicates the magnitude limit reached by the (combined) exposure in the header keyword ABMAGLIM. The value is calculated as the AB magnitude of a point-like source that has flux equal to 5 times the rms background and point-spread-function equal to the seeing (as reported in the header keyword SKY_RES). The actual computation was carried on using the recipe hdrldemo_maglim, available at https://ftp.eso.org/pub/dfs/pipelines/hdrl/). We computed also the median signal-to-noise (SNR) per pixel in the central 1" , at $R_{25}/4$ (R_{25} as reported in Table 1) and at $R_{25}/2$. This is calculated considering all the spectra within a circular annulus of radius $R_{25}/4$ and width 2" (e.g. $R_{25}/4$ +/- 1", similarly for $R_{25}/2$). The SNR calculation of each spectrum is done using the det_snr.py tool (https://www.stecf.org/software/ASTROsoft/DER_SNR/) in the wavelength range 4000 – 7000 angstrom. Table 2 summarizes for each target the "quality indicators" defined above. In addition, Table 2 reports the number of observations for each pointing and the exposure time for each expousure.

Spatial resolution

The average spatial resolution was measured by fitting a Gaussian function on a number of foreground stars sources in the white-lamp image over the entire field of view. These values are reported in the fits header keyword SKYRES. We also obtained a more precise measurement of the spatial resolution for the central pointings only, by fitting a Moffat function to the image of the Planetary Nebulae obtained using their [O III] emission line (Spriggs et al. 2020). We report this value in Table 2.

Ancillary files

Each datacube comes with an ancillary file, obtained by averaging the data cube along the wavelength direction (so called: white-lamp image). Figure 1 shows the white-lamp images of the target galaxies.

TARGET	SNR 1"	SNR R_{25} /4	SNR R_{25}/2	$PSF_{Centrer}$ [arcsec]	Mag $_{LIM}$	Center	Middle	Halo
FCC083	91	18	8	1.05	22.5	5x720	...	9x600
FCC090	37	15	7	1.00	23.6	5x720	...	3x600
FCC113	8	5	3	--	23.1	4x900	...	...
FCC119	17	11	7	0.94	24.0	5x720	...	3x600

FCC143	53	25	12	1.03	23.9	5x720	...	3x600
FCC147	137	34	17	1.29	22.6	5x720	...	9x600
FCC148	51	16	7	0.95	23.6	5x720	...	9x600
FCC153	38	10	3	0.89	23.6	5x720	...	9x600
FCC161	85	14	6	0.90	22.3	5x720	...	9x600
FCC167	99	25	10	0.93	22.5	5x720	6x600	9x600
FCC170	93	19	4	1.03	23.3	5x720	...	12x600
FCC176	30	10	6	--	22.2	4x900	...	...
FCC177	40	16	5	0.95	24.3	5x720	...	9x600
FCC179	74	17	8	--	22.6	4x900	...	4x900
FCC182	28	13	5	1.04	23.3	5x720	...	3x600
FCC184	142	39	18	1.23	23.9	5x720	6x600	9x600
FCC190	42	28	16	1.32	23.2	5x720	...	9x600
FCC193	90	31	11	0.90	24.1	5x720	...	9x600
FCC219	138	29	13	1.02	22.0	5x720	...	9x600
FCC249	82	33	16	1.14	23.3	5x720	...	3x600
FCC255	33	13	5	0.97	23.3	5x720	...	3x600
FCC263	24	13	6	1.00	22.3	4x900	...	...
FCC276	116	25	11	1.16	22.4	5x720	...	9x600
FCC277	44	26	11	1.05	22.6	5x720	...	3x720
FCC285	4	3	2	1.00	21.3	4x900	...	...
FCC290	43	18	12	1.00	21.3	4x900	...	4x900
FCC301	40	14	11	0.95	22.8	5x720	...	3x600
FCC306	9	7	5	1.00	22.9	4x900	...	...
FCC308	20	8	4	1.00	23.3	4x900	...	4x900
FCC310	45	21	9	0.95	23.4	5x720	...	9x600
FCC312	30	7	4	1.00	22.7	4x900	4x900	4x900

Table 2: Quality indicators for our target galaxies (see text for details). Column 1: target name. Columns 2-4: the median signal to noise ratio per pixel of the spectra observed within 1" (Col 2), within $R_{25}/2$ (Col 3), and $R_{25}/4$ (Col 4). The value of R25 for each galaxy is provided in Table 1. Column 5: the FWHM of the point-spread-function for the central pointings only, measured using the detected Planetary Nebulae. Column 6: magnitude limit in the AB photometric system of the exposures. Columns 7-9. Total exposure time for central, middle, and outer pointing (in form of of number_of_observations x exposure_time_per_observation, in units of seconds). The single central pointing of FCC 113, FCC 176, FCC 263, FCC 285, and FCC 306 covers also the outskirts of these galaxies.

Data Format

Files Types

The data for each target listed in Table 1 consist of a datacube and a a so-called white-lamp image, i.e. the average of the datacube along the wavelength direction. Each file, either datacube or associated image, are in FITS format. The basic information are stored in the primary header of the file, which is followed by a DATA extension. Errors are not included in the release.

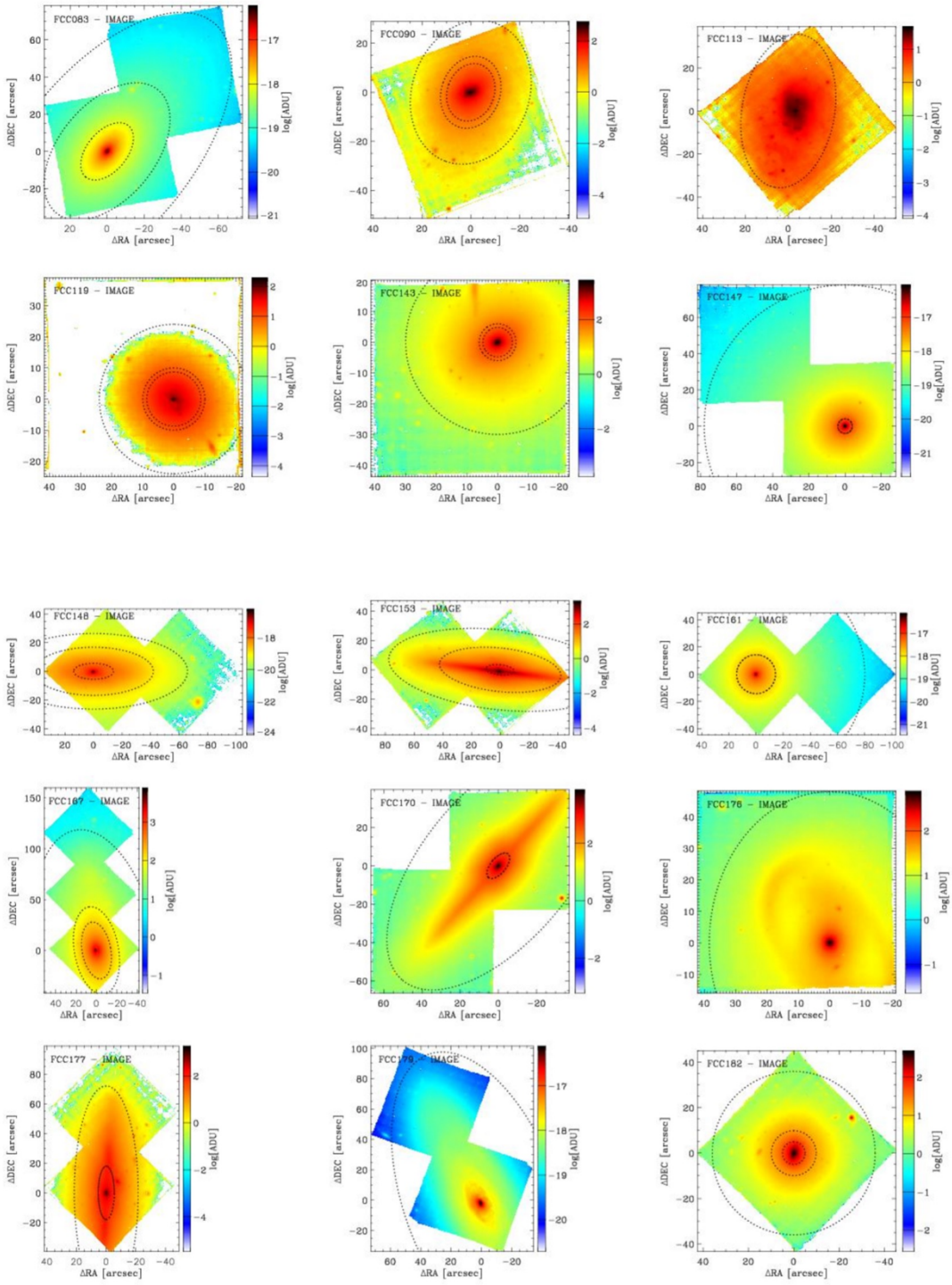

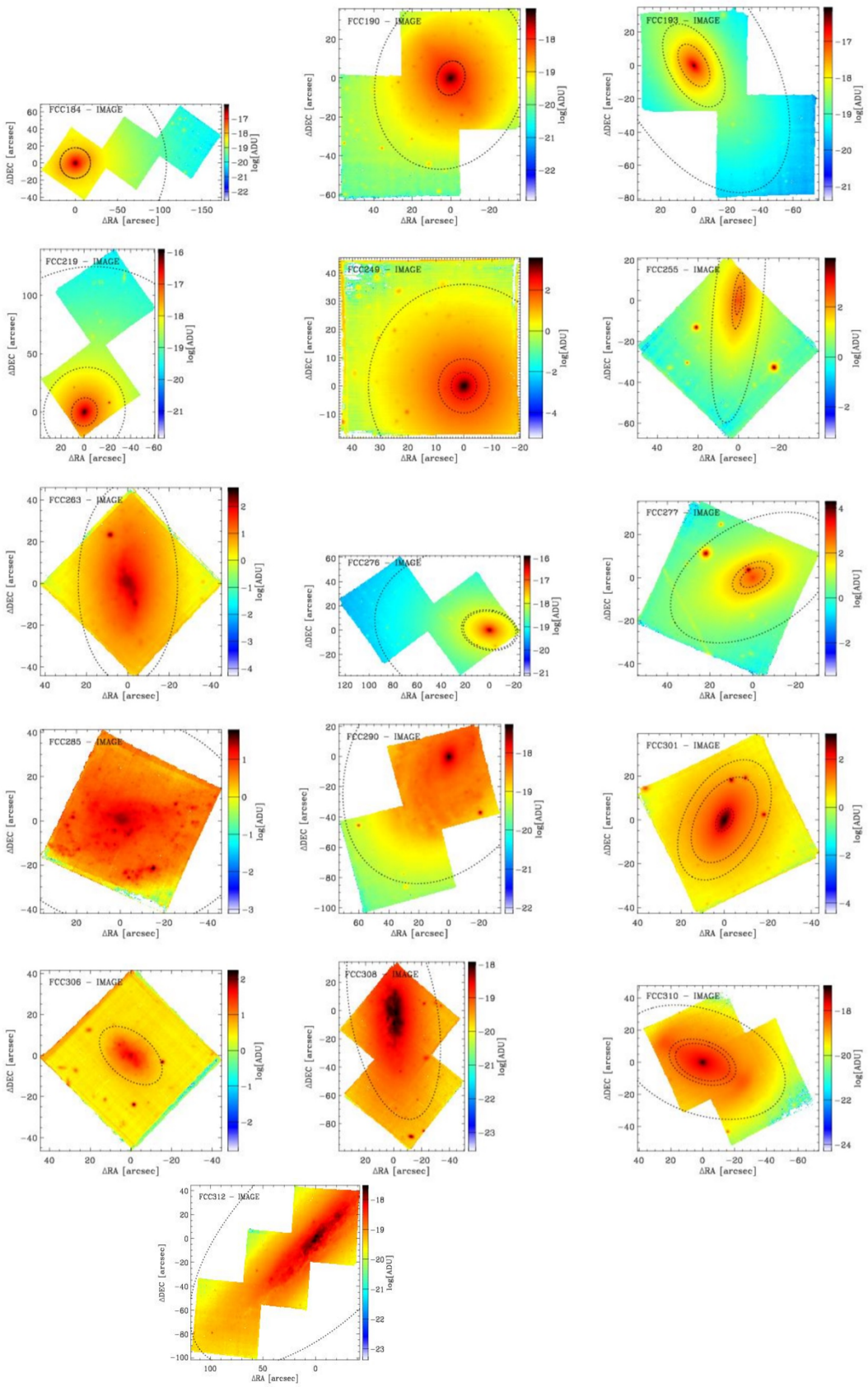

Figure 1. White-lamp image reconstructed from the data cube. The dashed ellipses show the 0.5 Re, R_{tr} (transition radius), and isophote at surface brightness 25 mag arcsec^{-2}. Note: not all ellipses are visible in all the fields of view. The transition radius (R_{tr}, i. e.: the radius at which the surface brightness profile is discontinuous, showing the transition between the contribution of halo light component and galaxy light component) is taken from Iodice et al. (2019).

Acknowledgements

The F3D scientific publications based on DR1 data are:

1. Fahrion K., et al., 2020a, A&A, 637, A26, *"The Fornax 3D project: Globular clusters tracing kinematics and metallicities".*
2. Fahrion K., et al., 2020b, A&A, 637, A27, *"The Fornax 3D project: Non-linear colour-metallicity relation of globular clusters".*
3. Galán-de Anta P. M., et al., 2021, A&A, 652, A109, *"The Fornax 3D project: PNe populations and stellar metallicity in edge-on galaxies".*
4. Iodice E., et al., 2019, A&A, 627, A136, *"The Fornax3D project: Tracing the assembly history of the cluster from the kinematic and line-strength maps".*
5. Lara-López M. A., et al., 2022, A&A, 660, A105, *"The Fornax3D project: The environmental impact on gas metallicity gradients in Fornax cluster galaxies".*
6. Martín-Navarro I., et al., 2019, A&A, 626, A124, *"Fornax 3D project: a two-dimensional view of the stellar initial mass function in the massive lenticular galaxy FCC 167".*
7. Martín-Navarro I., et al., 2021, A&A, 654, A59, "*Fornax 3D project: Assessing the diversity of IMF and stellar population maps within the Fornax Cluster".*
8. Pinna F., et al., 2019a, A&A, 623, A19, *"The Fornax 3D project: Unveiling the thick disk origin in FCC 170; possible signs of accretion".*
9. Pinna F., et al., 2019b, A&A, 625, A95, *"The Fornax 3D project: Thick disks in a cluster environment".*
10. Poci A., et al., 2021, A&A, 647, A145, *"The Fornax3D project: Assembly histories of lenticular galaxies from a combined dynamical and population orbital analysis".*
11. Poci A., et al., 2022, MNRAS, 514, 3660, *"The Fornax3D project: intrinsic correlations between orbital properties and the stellar initial mass function".*
12. Sarzi M., et al., 2018, A&A, 616, A121, *"Fornax3D project: Overall goals, galaxy sample, MUSE data analysis, and initial results".*
13. Spavone M., et al., 2022, A&A, 663, A135, *"Fornax3D project: Assembly history of massive early-type galaxies in the Fornax cluster from deep imaging and integral field spectroscopy".*
14. Spriggs T. W., et al., 2020, A&A, 637, A62, *"Fornax 3D project: Automated detection of planetary nebulae in the centres of early-type galaxies and first results".*
15. Spriggs T. W., et al., 2021, A&A, 653, A167, *"The Fornax3D project: Planetary nebulae catalogue and independent distance measurements to Fornax cluster galaxies".*
16. Viaene S., et al., 2019, A&A, 622, A89, *"The Fornax 3D project: dust mix and gas properties in the centre of early-type galaxy FCC 167".*
17. Zabel N., et al., 2020, MNRAS, 496, 2155," AlFoCS *+ Fornax3D: resolved star formation in the Fornax cluster with ALMA and MUSE".*
18. Zabel N., et al., 2021, MNRAS, 502, 4723," AlFoCS + F3D - II. Unexpectedly low gas-to-dust ratios in the Fornax galaxy cluster *AlFoCS + Fornax3D: resolved star formation in the Fornax cluster with ALMA and MUSE"*
19. Zhu L., et al., 2022, A&A, 664, A115, *"The Fornax3D project: Discovery of ancient massive merger events in the Fornax cluster galaxies NGC 1380 and NGC 1427".*

Data products of DR1 are created from observations collected at the European Organisation for Astronomical Research in the Southern Hemisphere under the following ESO programme: 296.B-5054(A).

Any publication making use of this data, whether obtained from the ESO archive or via third parties, must include the following statement in a footnote or in the acknowledgement:

> *Based on data obtained from the ESO Science Archive Facility with DOI: https://doi.org/10.18727/archive/82*

Publications making use of this data and which have been assigned an archive request number (of the form XXXXXX) must include the following statement in a footnote or in the acknowledgment:

> *Based on data obtained from the ESO Science Archive Facility under request number <request_number>.*

References cited in text:

- Bacon, R., Accardo, M., Adjali, L., et al., 2010, SPIE, 7735, 8. "*The MUSE second-generation VLT instrument*".
- Caon, N., Capaccioli, M., D'Onofrio, M. 1994, A&A, 106, 199. "*Global mapping B-band photometry of a complete sample of Fornax and Virgo early-type galaxies*."
- de Vaucouleurs, G., de Vaucouleurs, A., Corwin, H., G., et al. 1991 *"Third reference catalogue of bright galaxies (Vol 3)". (New York, NY: Springer).*
- Drinkwater, M., Gregg, M., D., Cikkessm M., ApJ, 548, 159. "*Substructure and dynamics of the Fornax cluster*".
- Ferguson, H., C., & Sandage, A., 1989, ApJ, 346, 53. *"The spatial distributions and intrinsic shapes of dwarph elliptical galaxies in the Virgo and Fornax clusters".*
- Freudling, W., Romaniello, M., Bramich, D., 1013, A&A, 559, 96. *"Automated data reduction workflows for astronomy. The ESO Reflex environement".*
- Iodice E., Spavone M., Capaccioli M., Peletier R., et al. 2019, A&A, 623, 1. "*The Fornax Deep Survey with VST. V. Exploring the faintest regions of the bright early-type galaxies inside the virial radius* ."
- Iodice, E., Sarzi, M., Bittner, A., et al., 2019, A&A, 627, A136, *"The Fornax3D project: Tracing the assembly history of the cluster from the kinematic and line-strength maps".*
- Sarzi, M. Iodice, E., Coccato, L., et al., 2018, A&A, 616, A121, *"Fornax3D project: Overall goals, galaxy sample, MUSE data analysis, and initial results".*
- Soto, K., T., Lilly, S., J., Bacon, R., et al. 2016, MNRAS, 458, 3210. *"ZAP – enhanced PCA sky sububtraction for integral field spectroscopy."*
- Spriggs T. W., et al., 2020, A&A, 637, A62, *"Fornax 3D project: Automated detection of planetary nebulae in the centres of early-type galaxies and first results".*
- Weilbaker, P., M., Streicher, O., Urrutia, T., 2012, SPIE, 8451, 08, *"Design and capabilities of the MUSE data reduction software and pipeline".*